An innovative geodesic based multi-valued fiber-tracking algorithm for diffusion tensor imaging

Sepasian, N.; Vilanova Bartroli, A.; ten Thije Boonkkamp, J.H.M.; ter Haar Romenij, B.M.

EINDHOVEN UNIVERSITY OF TECHNOLOGY
Department of Mathematics and Computer Science

An innovative geodesic based multi-valued fiber-tracking
algorithm for diffusion tensor imaging

by

N. Sepasian, A. Vilanova, J.H.M. ten Thije Boonkkamp,
B.M. ten Haar Romeny

An Innovative Geodesic Based Multi-Valued Fiber-Tracking Algorithm for Diffusion Tensor Imaging

N. Sepasian[a], A.Vilanova[a], J.H.M. ten Thije Boonkkamp[b], B. M. Ter Haar Romeny[a]

[a]*Department of Biomedical Engineering, Eindhoven University of Technology,*
PO Box 513, 5600 MB Eindhoven, The Netherlands
[b]*Department of Mathematics and Computer Science, Eindhoven University of Technology,*
PO Box 513, 5600 MB Eindhoven, The Netherlands

Abstract

We propose a new geodesic based algorithm for fiber tracking in diffusion tensor imaging data. Our algorithm computes the multi-valued solutions from the Euler-Lagrange form of the geodesic equations. Compared to other geodesic based approaches, multi-valued solutions at each grid point are computed rather than just computing the viscosity solution. This allows us to compute fibers in a region with sharp orientation, or when the correct physical solution is not the fiber computed from the first arrival time. Compared to the classical stream-line approach, our method is less sensitive to noise, since the complete tensor is used. We also compare our algorithm with the Hamilton-Jacobi equation (HJ) based approach. We show that in the cases where U-shaped bundles appear, our algorithm can capture the underlying fiber structure while other approaches may fail. The results for synthetic and real data are shown for both methods.

Keywords: Geodesic, Diffusion tensor images, Fiber tracking, Hamilton-Jacobi equation, Euler-Lagrange equations.

1. Introduction

Diffusion tensor imaging (DTI) is the only non-invasive technique that allows the reconstruction of brain white matter bundles [1, 2]. Due to the fibrous structure of white matter, diffusion of water molecules is dominant in the direction of the fibers. Diffusion and its directional variation can be measured by diffusion weighed magnetic resonance imaging(DW-MRI). By acquiring DW images in at least six gradient directions, it is possible to estimate a 3×3 symmetric matrix, the so-called diffusion tensor [1, 3]. The eigenvector corresponding to the largest eigenvalue of these tensors is considered to point in the direction of fiber tracts. Numerous algorithms have been introduced for reconstructing the fibrous structure from DTI. In the classic fiber tracking algorithm, the fibers are estimated by using the principal direction of the diffusion tensor. Here, fiber tracking stops if there is a sharp turn in the trajectory or when the fiber enters a region of low anisotropy, where the main eigenvector cannot be clearly identified. This can either be due to noise, or to the presence of crossing fibers. Furthermore, these methods are based on local characteristics and therefore sensitive to noise.

A possible solution to resolve these limitations of classic fiber tracking, is to apply more global approaches such as geodesic based algorithms [4, 5, 6, 7]. These techniques are based on the assumption that fibers follow the most efficient diffusion propagation paths. A Riemannian manifold is defined using as metric the inverse of the diffusion tensor. Paths in this manifold are shorter if the diffusion is larger along that path. Therefore geodesics (i.e., shorter paths) in this manifold follow the most efficient diffusion paths. The geodesics are often solved by using the stationary Hamilton-Jacobi equation (HJ). Equidistant fronts are described from a certain initial point. The propagation speed of the fronts at each point of the space is defined as a function of the local speed. Parker *et al.* [4] presented similar approaches where the

local speed was based on the combination of the normal vector and the tensor dominant eigenvector which defined the front propagation. This approach is prone to incorrect propagation in anisotropic domains. In recent publications [5, 6, 8], front propagation inside anisotropic domains has been considered, which is suitable for oriented domains . The propagation speed of the front is given by the diffusivity rate in the normal direction of the front; the fibers are extracted by back tracing the characteristics of the front.

One characteristic of solving the HJ-equation is that it gives only a single-valued viscosity solution corresponding to the minimizer of the length functional. It is also well known that the solution of the HJ-equation can develop discontinuities in the gradient space. These discontinuities occur when the correct solution becomes multi-valued. Therefore, developing an algorithm that can tackle these short comings becomes relevant. Parker *et al.* [9] show that some structures (e.g., Broca and Wernicke) have multiple path connections. Moreover, Jbabdi *et al.* [8] show that U-shaped fibers corresponding to the short association tracts cannot be captured by HJ-based algorithms.

In order to understand better the problem occur in HJ approach we illustrate a simple sketch that greatly can describe the shortcuts; figure 1. Generally, in geodesic approaches the Riemannian length is minimized. Using the inverse of the diffusion tensor leads the front propagate along the direction where the diffusion is higher. This can give the correct fiber if the anisotropic profile is nicely defined from the rest of the background; e.g. figure 1a. But in realistic examples usually this will not happen and in this case the two given points *a* and *b* can connect with the shortcut rather than the true fiber tracts. It is because considering the geodesic connecting to given points only as the function of space, then the geodesic will be a unique path that connecting the two given points. However, in the case when we have the directional domain; e.g. DTI space, geodesics also can be considered as a unique pathways connecting two given point with the given direction.
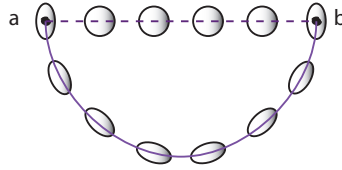

Figure 1: Comparison between geodesics in Riemannian and Euclidean space connecting *a* and *b*.

Recently, Sepasian *et al.* [10, 11] presented a ray-tracing based algorithm for computing geodesics in an anisotropic domain. This approach can capture multi-valued geodesics connecting two given points by considering the geodesics as the function of position and direction. Moreover, it is based on the Euler-Lagrange (EL) equations, and therefore local changes in the geodesic can be accounted for. However, in both papers, only synthetic data has been considered. We extend this method to 3D and compare our results with compatible numerical solution of HJ-equation. We make an initial evaluation of the methods on synthetic tensor fields and human diffusion tensor data. For the HJ approach, we use directly the stationary HJ-equation corresponding to the length functional minimizing the diffusivity rate along the geodesic. To solve this PDE we propose to apply iterative fast sweeping which is faster than other proposed algorithms such as fast marching. Fast sweeping is also more suitable for oriented domains [6, 12]. Once all geodesics are computed, one can filter out weak connections, using existing connectivity measures [10, 13].

In the following we first describe different mathematical models for computing geodesics and their connections to diffusion tensor images. Later, we propose the numerical methods for solving the respective equations. At last we present results for realistic synthetic data and human brain DTI.

2. Mathematical Models

As mentioned in Section 1, we assume that fiber tracts coincide with geodesics in the Riemannian manifold defined using the inverse of the diffusion tensor as metric. The intuition behind this assumption is that water molecules move freely along fiber tracts, and their movement is restricted in the perpendicular direction. Therefore, it is assumed that the fiber connecting two points follows the most efficient diffusion path for water molecules. We are searching for a path that maximizes diffusion. This can be achieved by inverting the metric that makes the largest eigenvalue become the smallest one. Consequently, the geodesic

as a function of this metric represents the fibers [14]. In order to construct the geodesics, two different classes of governing equations can be derived. In this section, first we present the Euler-Lagrange(EL) equation for a specific metric. Next, we formulate the corresponding Hamilton-Jacobi(HJ) equation and its relation to EL equation.

Consider a bounded curve C, with parametrization $\boldsymbol{x} = \chi(\tau)$, $a \leqslant \tau \leqslant b$. A geodesic between two points $\chi(a)$ and $\chi(b)$ is the smooth curve whose length is the minimum of all possible lengths. In the presentation that follows we use the Einstein notation, i.e., we sum over repeated indices, in the upper (superscript) and in the lower (subscript) position. Introducing the metric $\mathrm{d}s^2 = g_{\alpha\beta}\mathrm{d}x^\alpha \mathrm{d}x^\beta$, the length of C is given by

$$J[\chi] = \int_C \mathrm{d}s = \int_a^b \left(g_{\alpha\beta}(\chi(\tau))\, \dot{\chi}^\alpha(\tau)\dot{\chi}^\beta(\tau) \right)^{1/2} \mathrm{d}\tau, \tag{1}$$

where $G = (g_{\alpha\beta})$ is the inverse of the diffusion tensor D, i.e., $G = D^{-1}$. Therefore, $(g_{\alpha\beta})$ only depends on $\boldsymbol{x}$, and is symmetric positive definite. In the following we use the short hand notation $\dot{x}^\alpha = \dot{\chi}^\alpha(\tau)$.

From calculus of variations, we know that the necessary condition for $\chi(\tau)$ to minimize $J[\chi]$ is the set of Euler-Lagrange equation which lead [15]

$$\frac{\partial L}{\partial x^\alpha} - \frac{d}{d\tau}\left(\frac{\partial L}{\partial \dot{x}^\alpha} \right) = 0, \tag{2}$$

where $L = L(\boldsymbol{x}, \dot{\boldsymbol{x}})$ is the Lagrangian corresponding to (1) and is given by

$$L(\boldsymbol{x}, \dot{\boldsymbol{x}}) = \left(g_{\alpha\beta}(\boldsymbol{x})\dot{x}^\alpha \dot{x}^\beta \right)^{1/2}. \tag{3}$$

The required derivatives of L are given by

$$\frac{\partial L}{\partial x^\alpha} = \frac{1}{2L}\frac{\partial g_{\beta\gamma}}{\partial x^\alpha}\dot{x}^\beta \dot{x}^\gamma, \quad \frac{\partial L}{\partial \dot{x}^\alpha} = \frac{1}{L}g_{\beta\alpha}\dot{x}^\beta.$$

Next we take for τ the arc length, i.e., if $L = 1$ then $\frac{\mathrm{d}L}{\mathrm{d}\tau} = 0$ [16]. Substituting the derivatives above in (2), we obtain,

$$g_{\alpha\beta}\ddot{x}^\beta + [\beta\gamma, \alpha]\dot{x}^\beta \dot{x}^\gamma = 0, \tag{4}$$

where $[\beta\gamma, \alpha]$ is the Christoffel symbol of the first kind, given by,

$$[\beta\gamma, \alpha] = \frac{1}{2}\left(\frac{\partial g_{\alpha\beta}}{\partial x^\gamma} + \frac{\partial g_{\alpha\gamma}}{\partial x^\beta} - \frac{\partial g_{\beta\gamma}}{\partial x^\alpha} \right); \tag{5}$$

see [17, 15]. Multiplying (4) with the inverse of the metric $G^{-1} = (g^{\alpha\beta})$, we find

$$\ddot{x}^\alpha + \Gamma^\alpha_{\beta\gamma}\dot{x}^\beta \dot{x}^\gamma = 0, \tag{6}$$

where $\Gamma^\alpha_{\beta\gamma}$ is the Christoffel symbol of the second kind, defined by

$$\Gamma^\alpha_{\beta\gamma} = g^{\alpha\delta}[\beta\gamma, \delta]. \tag{7}$$

Consider the functional that minimizes the length of all curves joining $\chi(a)$ and $\chi(t)$

$$T(\boldsymbol{x}, t) = \min \int_a^t L(\chi(\tau), \dot{\chi}(\tau))\mathrm{d}\tau, \tag{8}$$

with $\boldsymbol{x} = \chi(t)$ and L given in (3), i.e., the upper bound is variable.

The geodesic connecting $\chi(a)$ with $\chi(t)$ can be determined from the Hamilton-Jacobi equation, given by [18]

$$H\left(\boldsymbol{x}, \frac{\partial T}{\partial \boldsymbol{x}} \right) = 1, \tag{9}$$

where [18, 19]

$$H^2(\boldsymbol{x}, \boldsymbol{p}) = g^{\alpha\beta}(\boldsymbol{x})p_\alpha p_\beta \quad p_\alpha := g_{\alpha\beta}(\boldsymbol{x})\dot{x}^\beta, \tag{10}$$

3

With this choice for the Hamitonian we obtain the *anisotropic eikonal* equation

$$F(x^\alpha, q_\alpha) = g^{\alpha\beta} \frac{\partial T}{\partial x^\alpha} \frac{\partial T}{\partial x^\beta} - 1 = 0 \qquad q = \frac{\partial T}{\partial x^\alpha}. \qquad (11)$$

We can show that the first order PDE (11) is equivalent to the Charpit's system of equations [20], i.e.,

$$\dot{x}^\alpha = \frac{\partial F}{\partial q_\alpha} = g^{\alpha\beta} q_\beta, \qquad (12a)$$

$$\dot{q}^\alpha = -\frac{\partial F}{\partial x^\alpha} = -\frac{1}{2} \frac{\partial g^{\beta\gamma}}{\partial x^\alpha} q_\beta q_\gamma, \qquad (12b)$$

$$\dot{T} = q_\alpha \frac{\partial F}{\partial q_\alpha} = g^{\alpha\beta} q_\alpha q_\beta. \qquad (12c)$$

This 7-dimensional system of ODEs describes the solution of (11). Here (12a) and (12b) are the canonical form for EL equations.

The solution of the HJ equation may develop multi-valued solutions when two fronts collide, i.e., such as focus points, caustics and discontinuities in the gradient field. Those regions are called *shocks*. Therefore, the viscosity solution is needed to ensure the existence and uniqueness of the solution to equation (11); see e.g., Mantegazza and Mennucci [21]. However, using the viscosity solution will not ensure that the solution we obtain is the real physically meaningful solution [22]. In fact, we will see in Section 5 that the solutions we obtain are not always the desired ones.

In DTI fiber tracking, different methods have been derived based on front propagation in the anisotropic fields using the HJ-equation. Jackowski *et al.* [6] introduced the Hamiltonian that minimizes conformal energy rather than computing the geodesics [16]. The reason is basically because the Hamiltonian depends on the diffusion tensor rather than its inverse. Since our main focus is on geodesic based minimization approach we turn our focus to this class of methods. Another well-known approach is presented by Parker *et al.* [4] and Lenglet *et al.* [23]. In these publications they derived the time dependent form of HJ equation by minimizing the energy functional. It is more convenient and less computationally expensive to model our problem with the steady HJ-equation.

Note that equation (11) is obtained by means of a variational formulation that considers the entire domain and complete data to calculate the optimal curves. The resulting optimal paths will be those that globally minimize the cost, thus obtaining those minimizing the diffusion along the trajectory. This method is a global minimization approach and thereby more robust to noise than more local based methods and can connect the initial point to any point inside the domain. However, Jbabdi *et al.* [8] showed that the choice of metric and the numerical method can result in shortcuts if tensors are not sharp enough.

Sepasian *et al.* [10, 11] introduced a new algorithm based on the ray-tracing method for geodesic fiber tracking. In this approach all arrival times of the fronts are considered rather than only fixing the first arrival time at each grid points. The major advantage of this approach is the capability of capturing possible multi-path connections between two given points. However, these papers by Sepasian *et al.* were presented only for unrealistic synthetic data fields. The motivation of this paper is to extend and evaluate a similar algorithm for capturing the multi-valued geodesic for 3D synthetic data and human brain DTI.

3. Numerical Methods

In this section we focus on constructing numerical schemes for computing numerically the geodesics using geodesic equations (6) and HJ-equation (11). First, we present the so-called ray-tracing method for reconstructing fiber tracts in a 3D Riemannian space. Subsequently, we explain the numerical discritization and algorithm for computing the solution of the HJ equation.

3.1. Ray Tracing

A geodesic connecting a pair of points on a Riemannian manifold is minimizing the length functional (1). Let $\boldsymbol{x} = (x^1, x^2, x^3)^\top$ be a point on a geodesic. As we showed in Section 2, the minimizer of (1) satisfies

the system of three second order ODEs (6) with so-called Christoffel symbols defined in (5) and (7). Let us introduce $u^\gamma(\tau) := \dot{x}^\gamma(\tau)$ for $\gamma = 1, 2, 3$, then we can rewrite system (6) as follows

$$
\begin{aligned}
\dot{x}^\alpha &= u^\alpha, \\
\dot{u}^\alpha &= -\Gamma^\alpha_{\beta\gamma} u^\beta u^\gamma.
\end{aligned}
\tag{13}
$$

Consider a point $(x^1(0), x^2(0), x^3(0))$ as the given initial point in the domain and $(u^1(0), u^2(0), u^3(0))$ as initial direction. We compute the solution to (13) for the given initial position and multiple initial directions using sophisticated ODE solvers, such as the fourth order explicit Runge-Kutta method. This gives us a set of geodesics connecting the given initial point to some points on the boundary.

The computational domain is discretized uniformly with grid size h and grid points $x_{ijk} = (x^1_i, x^2_j, x^3_k) = h(i, j, k)$ for $i = 0, 2, 3, \ldots, N-1$, where N is number of grid points in each spatial direction. For simplicity we take the number of grid points equal in all directions. We assign to each grid point with a 3×3 tensor $G_{ijk} = D^{-1}_{ijk}$.

We approximate the derivatives of $g_{\alpha\beta}$ at each grid point by the standard second order central difference scheme, i.e.,

$$
\frac{\partial g_{\alpha\beta}}{\partial x^1}(x^1_i, x^2_j, x^3_k) \approx \frac{1}{2h}\left(g_{\alpha\beta}(x^1_{i+1}, x^2_j, x^3_k) - g_{\alpha\beta}(x^1_{i-1}, x^2_j, x^3_k)\right).
\tag{14}
$$

Second order one-sided differences are applied when the grid points are situated on the boundary, i.e,

$$
\frac{\partial g_{\alpha\beta}}{\partial x^1}(x^1_0, x^2_j, x^3_k) \approx
\tag{15}
$$
$$
\frac{1}{2h}\left(-3g_{\alpha\beta}(x^1_0, x^2_j, x^3_k) + 4g_{\alpha\beta}(x^1_1, x^2_j, x^3_k) - g_{\alpha\beta}(x^1_2, x^2_j, x^3_k)\right),
$$
$$
\frac{\partial g_{\alpha\beta}}{\partial x^1}(x^1_{N-1}, x^2_j, x^3_k) \approx
\tag{16}
$$
$$
\frac{1}{2h}\left(3g_{\alpha\beta}(x^1_{N-1}, x^2_j, x^3_k) - 4g_{\alpha\beta}(x^1_{N-2}, x^2_j, x^3_k) + g_{\alpha\beta}(x^1_{N-3}, x^2_j, x^3_k)\right).
$$

Note that similar expressions hold for derivatives with respect to x^2 and x^3. Solving the ODE system gives the solution at points that are not necessarily located in the grid points. Therefore, the value of the metric and its derivatives are obtained by applying trilinear interpolation at any grid point at the domain where the value of metric is not available. Initial vectors are uniformly distributed using the vertices of regular symmetrical polyhedra [24]. The integration of geodesics continues until the geodesic hits the boundary of the computational domain.

3.2. Fast Sweeping

To discretize a general Hamiltonian $H(x, p)$ several techniques have been developed for both structured and unstructured meshes. In this paper we use the Lax-Friedrichs (LF) numerical discretization, proposed by Kao *et al.* in [25], which satisfies the required monotonicity and consistency conditions. The major motivation to apply the LF scheme is that an explicit solution formula will always be possible to derive without any assumption on the Hamiltonian.

In order to compute the solution of the descretized eikonal equation, a suitable numerical method needs to be applied. Lenglet *et al.* [23] and Jbabdi *et al.* [8] apply fast marching schemes used to estimate geodesics and the viscosity solution of the time-dependent HJ equation. Jackowski *et al.* [6] apply the fast sweeping scheme to estimate the viscosity solution of the stationary HJ-equation. In this approach short trajectories that minimize some conformal energy, corresponding to the largest diffusion along the trajectories, is estimated rather than the geodesics. Kao *et al.* [12] show that for computing the optimized trajectories using the fast sweeping scheme, regardless of discritization, gives the cheapest computational complexity. Therefore, in this paper we also focus on the fast sweeping scheme for computing the geodesics.

We start with the derivation of an explicit formula for the 3-dimensional eikonal equation (11). First we introduce the difference approximations

$$
\begin{aligned}
\delta_{x^1} T_{ijk} &:= \frac{1}{2h}\left(T_{i+1,j,k} - T_{i-1,j,k}\right), \\
\delta_{x^1 x^1} T_{ijk} &:= \frac{1}{h^2}\left(T_{i+1,j,k} - 2T_{i,j,k} + T_{i-1,j,k}\right),
\end{aligned}
\tag{17}
$$

5

and the averaging operator

$$\mu_{x^1} T_{ijk} = \frac{1}{2} \left(T_{i+1,j,k} + T_{i-1,j,k} \right), \tag{18}$$

and likewise for operators in x^2 and x^3. At each mesh point $\boldsymbol{x}_{ijk}$ we have the following numerical approximation

$$H \left(\boldsymbol{x}_{ijk}, \delta_{x^1} T_{ijk}, \delta_{x^2} T_{ijk}, \delta_{x^3} T_{ijk} \right) \quad - \tag{19}$$
$$\frac{1}{2} h \left(\sigma_1 \delta_{x^1 x^1} T_{ijk} + \sigma_2 \delta_{x^2 x^2} T_{ijk} + \sigma_3 \delta_{x^3 x^3} T_{ijk} \right) \quad = \quad 1.$$

Notice that the only unknown in the equation above is T_{ijk}, which can be isolated to obtain the iterative solver

$$T_{ijk}^{n+1} = c \left(1 - H(\boldsymbol{x}_{ijk}, \delta_{x^1} T_{ijk}, \delta_{x^2} T_{ijk}, \delta_{x^3} T_{ijk}) \right) \tag{20}$$
$$+ \quad \frac{1}{2h} c T_{ijk} \left(\sigma_1 \mu_{x^1} + \sigma_2 \mu_{x^2} + \sigma_3 \mu_{x^3} \right),$$

where,

$$c = \frac{h}{\sigma_1 + \sigma_2 + \sigma_3}.$$

Here σ_1, σ_2 and σ_3 are the artificial viscosities satisfying,

$$\sigma_1 \geq \max \left| \frac{\partial H}{\partial p_\alpha} \right| = \max \left| g^{\alpha\beta} p_\beta \right|.$$

The iteration indices on T_{ijk} in the right hand side of formula (20) are omitted on purpose, since depending on the direction of the sweeping, the value will correspond to the previous calculation, or the current one. We can show that the monotonicity and convergence of the method is dependent on the appropriate choice of the viscosity terms σ and the grid size of the computational domain. To ensure monotonicity of the scheme, we want to keep the viscosity term as small as possible. There are different studies on the appropriate choice of value for viscosity terms and they show that there is a direct relation between convergence rate of the solution and viscosity term. In this paper we choose these values to be 1. More details about the convergence and accuracy of LF scheme is studied by authors [12, 26].

We solve the discretized system (20) using the discretized fast sweeping method. Fast sweeping relies on the idea of using central finite differences and Gauss-Seidel iteration with alternating sweeping directions. Dividing the characteristics into a finite number of groups according to their direction, the fast sweeping method follows the causality along characteristics. This means that the newly computed value, T_{ijk} only depends on the past values in grid points located in the direction of the characteristics of (11) through $\boldsymbol{x}_{ijk}$. As the method relies on the fact that by sweeping in different directions, the direction of the characteristic will be eventually followed, there is no need for sorting, in contrast to the fast marching method. The computational complexity of the algorithm is $O(N^3)$ for a total of N grid points in each direction and the number of iterations is independent of the grid size [27, 28, 29].

The fast sweeping algorithm consists of the following steps: initialization, alternating sweepings and enforcing boundary conditions.

Initialization. We assign the exact boundary condition to T_{ijk}^0 at the boundary and keep these values fixed during the iterations. At the interior points we set $T_{ijk}^0 = M$ with M larger than the maximum of the true solutions. These values will be updated in the process of iterations.

Gauss-Seidel Alternating Sweepings. At iteration $n + 1$, calculate T_{ijk}^{n+1} that solves equation (20). At all grid points $\boldsymbol{x}_{ijk}$ in the internal domain we carry out the Gauss-Seidel iteration except in those that have a local converged solution value. Recall that this process has to be done in alternating sweeping directions, i.e., opposite diagonal directions.

Enforcing Boundary Conditions. After each sweep, we enforce boundary conditions to ensure that characteristics flow outside the domain and error cannot propagate into the domain.

Convergence Test. After all the sweepings are performed, check whether:

$$\| T^{n+1} - T^n \|_{L_1} \le \epsilon. \tag{21}$$

where $\epsilon > 0$ is the convergence tolerance.

The computational domain of the method is bounded. Therefore, in order to avoid propagation of errors from the boundary to the interior domain, we have to impose special boundary condition. Therefore, we have to specify carefully the values of points outside the computational domain, otherwise huge errors may be introduced and propagate into the computational domain. To tackle this problem, Kao *et al.* [25] propose the following condition in a two dimensional case easily extendable to the higher dimension

$$\begin{cases} u_{0,j,k}^{\text{new}} = \min\left(\max\left(2u_{1,j,k} - u_{2,j,k}, u_{2,j,k}\right), u_{0,j,k}^{\text{old}}\right), \\ u_{N-1,j,k}^{\text{new}} = \min\left(\max\left(2u_{N-2,j,k} - u_{N-3,j,k}, u_{N-3,j,k}\right), u_{N-1,j,k}^{\text{old}}\right). \end{cases}$$

Note that the same condition can simply be written for other boundaries.

The optimal paths for the system described by the Hamiltonian, can be obtained by solving the Charpit's equations (12). Notice, that the momenta can be computed from the viscosity solution. For this we use the central difference scheme. one can construct the solution for the PDE (11), by integrating each one of these equations along t.

4. Pre and Post Processing

In the previous sections we described how to compute the geodesics in general. In the following we focus on pre and post processing suitable for our specific algorithms.

Pre-processing. All geodesic based methods allow the geodesics to deviate from the direction of diffusion. This is an advantage because they become less sensitive to noise, but at the same time the geodesics can deviate too much if diffusion profiles are not sharp. In order to deal with this problem, Descoteaux *et al.* [30] propose tensor sharpening by raising tensors to a certain power, i.e. where

$$D_{\text{sharp}} = D^n.$$

Where D and D_{sharp} are the diffusion tensor and sharpened tensor, respectively. This results diminishing the isotropic part and enhancing the dominant eigenvectors. However, powering the tensor can introduce other issues such as enhancing noise. The proper choice of the exponent n is highly depend on the data and its orientation and different values are proposed [30, 31].

Since the assessment of the anatomical correctness of the fiber tracts using sharpening in out of the scope of this paper, we leave real data tensors unchanged. Note that to be fair for evaluating all methods we present in this paper, we apply the tensor sharpening to all tensors inside the domain and no masking is applied.

Post-processing. Once all geodesics are computed, depending on the application and algorithm, two different post-processing approaches can be desirable.

- The first post-processing approach is applicable for the ray-tracing algorithm. It refers to applying the two-point ray tracing algorithm proposed in [32] and extended to 3D Riemannian space by Sepasian *et al.* [10] for computing the multi-valued geodesics between two given points inside the domain. First the geodesic equation are solved for these two given points as initial locations and discrete set of initial directions. This gives two sets of geodesics starting at these two points and ending at the boundary. The post-process of these solutions gives the geodesics between the two points [10, 33]. Note that finding the exact pathway connecting two given point is not valuable and realistic for DTI fiber-tracking. Therefore, in this paper we will not focus on this postprocessing.

- The second post-processing approach for ray-tracing algorithm is to apply region-region fiber-tracking. This can be done by selecting the regions of interests and filter all geodesics that pass through both selected regions. Note that geodesics are computed until they meet one of the boundaries. In order to only show the fiber connecting two given region we apply the line-plane intersection. This allows to stop the geodesics once they meet one of the selected regions.

- The last post-processing method is to measure the strength of geodesics connecting two points and can be applied for both algorithms. The connectivity measure is used for finding a suitable trajectory corresponding best to real fiber bundles. We apply these measures in order to discard the geodesics, which are not holding strong connections between points in the domain. Since the fibers correspond to the geodesics connecting a pair of points in the Riemannian manifold, the most reasonable connectivity measure is the one that minimizes trajectories in a Riemannian manifold.

In recent papers, Astola *et al.* [13] and Parker *et al.* [7] represent the connectivity measure as ratio of lengths given by the Euclidean and Riemannian metric tensors, respectively. This measure can be considered as a measure for the connectivity strength of a geodesic. The proposed measure reads

$$m[\chi] = \frac{\int_a^b |\dot{\chi}(\tau)|\mathrm{d}\tau}{J[\chi]}. \tag{22}$$

Note that locally, in anisotropic voxels, this measure obtains its maximum in the direction of the eigenvector corresponding to the largest eigenvalue; see Astola *et al.* [13].

5. Results

In this section we compute geodesics for a discrete three-dimensional synthetic tensor field and real human brain DTI. We present the result of the ray-tracing algorithm and our implementation of the fast-sweeping method.

5.1. Synthetic Data

We evaluate both geodesic methods using simulated tensor data. We want to demonstrate that our proposed ray-tracing method is superior to the fast sweeping method for fiber bundles with high curvature, like U-shaped fiber bundles.

Isotropic tensors are imposed as background, excluding the influence of noise. In order to mimic real DTI acquisition, Rician noise is added to a 20×20×6 synthetic image containing 1×1×1 mm voxels. To compute Rician noise, the signal attenuation is obtained using the inverse of the Stejskal-Tanner relation, see [34]. The noise is added to the noiseless diffusion tensors in each direction with signal to noise ratio(SNR) 15.3 Let us define the curved region as R_1 and the background as R_2, then tensors belonging to each region are computed with eigenvalues, $\lambda_{R1} \sim [3, 17, 17] \times 10^{-4}$ mm^2/s, and $\lambda_{R2} \sim [7, 7, 7] \times 10^{-4}$ mm^2/s. For pre-processing of the synthetic data experiments we choose the tensor sharpening factor $n = 2$.

Figure 2 shows the results for the U-shaped fiber obtained from the HJ-equation with different choices of end points in 2a and 2b, and from the ray-tracing algorithm 2c. The background is color coded based on the fractional anisotropy (FA) and fiber tracts are color coded using the dominant direction of the tensors. The initial points and seed points are visualized by black circles. The arrows in all images show the direction of fiber reconstruction. We see in ray tracing figure the two possible geodesics starting from the given initial point and meet at the same point at the other side of the U-fiber. Note that applying the connectivity measure (22) gives the higher value for the fiber following the U-fiber. Figures 2a and 2b display the problem of *shortcuts* that can occur in the HJ approach. Lenglet *et al.* [23] relate this error to the choice of metric as the inverse of the diffusion tensor. We show in figure 2c, with the same choice of metric and minimizing the same functional, that capturing the correct geodesic corresponding to the desired fiber bundle is feasible. A heuristic explanation is that the viscosity solution obtained via fast sweeping only gives the solution corresponding to the first arrival time. Since we apply no masking for defining the anisotropic region from an isotopic background, in the cases with more complex structure like U fibers, the Riemannian length of the wrong trajectory will win the cost of the front evolution resulting in the shortcut connecting the two
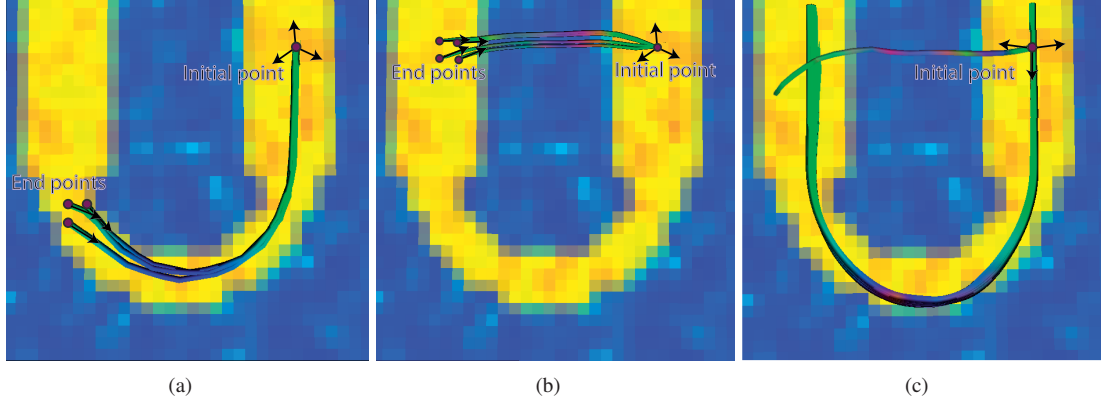
Figure 2: Geodesics computed by using the HJ-equation with different choices of end points (a,b) and the ray tracing algorithm (c). In all cases the initial value is situated in the same point.

head of the U. The mathematical model for providing the geodesic equation, considers the local changes inside the domain in ray racing better in comparison with HJ approach. This property has advantages and disadvantages: at one hand, it makes EL approach still local compare to HJ approach and more prone to noise sensitivities. On the other hand, thank to the same property, it gives us the possibility to capture the correct trajectory, to use the whole tensor information and to not be restricted to the main diffusion direction. However, as we mention and show in our results, here we only consider the classic ray-tracing method. The problem of local minimization is tackled once the model changes to two-point ray tracing introduced in [10, 22, 33].

In order to find the best corresponding fibreous structure, the geodesic is computed by shooting rays from an initial point to all possible directions. Using the connectivity measure (22) we select the strongest connection with the largest connectivity value. In figure (2)c, the largest connectivity measure belongs to the fiber following the U-fiber. Note that in figure 2c the small distortions from the optimal shooting vector still results in good approximations of the underlying fiber structure.

5.2. Real Data

We present a qualitative evaluation of the algorithms based on real data. The data set is acquired from a healthy subject using a Philips scanner, with $128 \times 128 \times 66$ voxels, with resolution $2 \times 2 \times 2$mm, b-factor of $1000 s/\text{mm}^{-2}$ and 16 gradient directions.

To show the potential of the ray-tracing method for real data, we evaluate it for various well-known fiber bundles including *Corpus Callosum* (CC) and *Superior Longitudinal Fasciculus* (SLF); see figure 3. In these example the seed points are selected manually in the DTI space. Here we only trace the geodesics in the direction of the main eigenvalue and small perturbation around the main eigenvector direction of the seed point. The tracing is stopped after a limited time and fiber are selected using the connectivity measurement (22). We see that fiber tracts constructed with our method in both region comply with the known anatomy of the white matter [3].

One of the interesting regions with more complex shaped fibers is the area around the *Thalamic Radiation* [35]. Figure 4 shows the result of the selected region obtained from stream-line method, fast sweeping and ray tracing, respectively. The rational behind selecting the *Thalamic Radiation* is the less defined diffusion directions in this region. Therefore, usually the tracts of interest are smaller or probably more entangled than major bundles like CC. In figure 4 the seed points are selected manually. For all algorithms the seed points are the same. Since the diffusivity is not well-defined in this region using stream-line method result in cutted fiber tracts, see figure 4a. The threshold used as stopping criteria in streamline method is the FA smaller than 0.3. We also apply the HJ approach and as we expect this method gives shortcuts as result compare to ray tracing approach, see figure 4b. In figure 4c we present the ray-tracing result where the shape is nicely followed. For 4b we perform the fast sweeping algorithm from the selected initial point. In
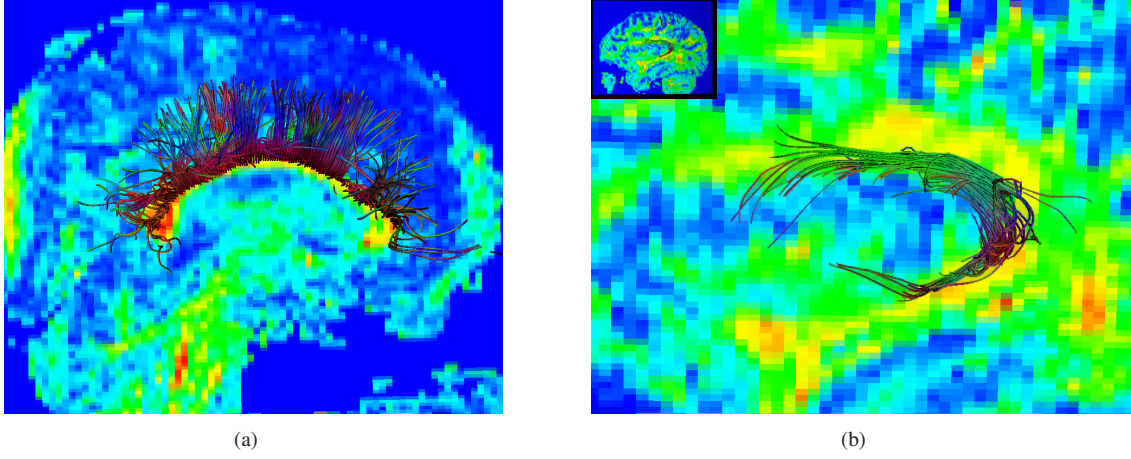
Figure 3: Ray tracing fiber-tracking for Corpus Callosum (a) and Superior Longitudinal Fasciculus (b).

order to construct the fibers we backtrack the characteristics from the selected endpoints. Since there is no ground truth in real data we present our results to the neuroanatomist to validate our findings. According to her observation the result in figure 4c agrees well to what is expected and the region selected corresponds with *Thalamic Radiation*.
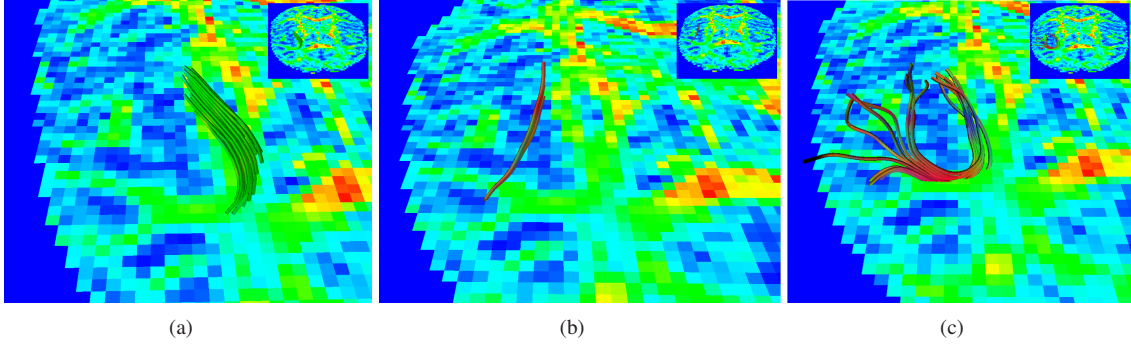

Figure 4: Fiber-tracking for short connection fibers in *Thalamic Radiation* using Stream-line(a), Geodesic using HJ equation (b) and Geodesic using ray-tracing method (c).

6. Conclusions and Future Work

In this paper, we have presented geodesic based methods for fiber tracking in diffusion tensor imaging. We presented the Euler-Lagrange geodesic equations for three-dimensional Riemannian space and applied the ray tracing method to compute the solution. This new algorithm allows us to have more control over local orientation inside the domain and gives multi-valued solution. Alternatively, We also discussed a fast sweeping algorithm as an example of the first arrival solvers to solve the the stationary form of HJ equation. Compare to the fast marching method proposed in other publications for solving HJ equation, fast sweeping has less computational costs and it is more suitable for oriented domains. However, the viscosity solution to this equation is not always the correct physical solution because it corresponds to the first arrival time only. This method and similar approaches are very robust to noise. However, they can produce nonphysical solutions,e.g. shortcut. It can be either due to the computation of the only first arrival time or the choice of the functional to be minimized. It is worthwhile to investigate the behavior of these class of methods

using different functionals. Assume the cost for going through the correct fiber tract is the ratio between the Riemannian and the Euclidean length of the trajectory, we show that in the HJ approach the fiber tracking will collapse when the Euclidean and Riemannian lengths are proportional. Therefore, it is very interesting to think about the functional that minimizes trajectories as not only the Riemannian length but also the ratio between Riemannian and Euclidean lengths. However, in general, HJ based methods are suitable for dealing with major fiber tracts and long associated fiber bundles.

Results for realistic synthetic data have been shown for both HJ based fiber tracking and our proposed ray tracing algorithm. We show the potential of our method for capturing the correct tract, especially the short associated fibers, i.e., U-shaped fibers.

The ray-tracing approach suffers from some drawbacks. This numerical scheme computes a finite number of rays; when these rays diverge, some regions will be visited by many rays and some by none. Controlling the ray density to achieve roughly uniform sampling of the travel-time is feasible by using some expensive interpolation, but is computationally expensive. The challenge is to devise an algorithm which retains the efficiency of modern first arrival time solvers and at the same time capture all arrival times. As an extension of this research, we are currently investigating the generalization of the ray-tracing algorithm for fiber tacking to higher resolution DTI, such as high angular resolution diffusion imaging. Furthermore, since fibers can be computed independently, the algorithm is highly suitable for parallel computations.

7. Acknowledgements

References

[1] Basser, P.J., Pierpaoli, C.: Microstructural and physiological features of tissues elucidated by quantitative-diffusion-tensor MRI. Journal of Magnetic Resonance **111**(1) (1996) 209–219

[2] Mori, S., Crain, B.J., Chacko, V., van Zijl, P.: Three-dimensional tracking of axonal projections in the brain by magnetic resonance imaging. Annals of Neurology **45** (1999) 265–269

[3] Mori, S., Wakana, S., van P. Zijl, Nagae-Poetscher, L.: MRI atlas of human white matter. (2005) Elsvier, Berlin (2005).

[4] Parker, G.J.M., Wheeler-Kingshott, C.A.M., Barker, G.J.: Distributed anatomical brain connectivity derived from diffusion tensor imaging. Information Processing in Medical Imaging, 17th International Conference **2482** (2001) 106–120

[5] Lenglet, A., Deriche, R., Faugeras, O.: Inferring white matter geometry from diffusion tensor MRI: application to connectivity mapping. Proceedings of the Eighth European Conference on Computer Vision **3021–3024** (2004) 127–140

[6] Jackowski, M., Kao, C., Qui, M., Constable, R., Staib, L.: White matter tractography by anisotropic wavefront evolution and diffusion tensor imaging. Medical Image Analysis **9** (2005) 424–440

[7] Prados, E., Soatto, S., Lenglet, C., Pons, J.P., Wotawa, N., Deriche, R., Faugeras, O., Soatto, S.: Control theory and fast marching techniques for brain connectivity mapping. IEEE computer society press **1**(1) (2006) 1076–1083

[8] Jbabdi, S., Bellec, P., Toro, R., Daunizeau, J., Pélégrini-Issac, M., Benali, H.: Accurate anisotropic fast marching for diffusion-based geodesic tractography. International Journal of Biomedical Imaging **2008** (2008) 1–12

[9] Parker, G., Luzzi, S., Alexander, D., Wheeler-Kingshott, C., Ciccarelli, O., Lambon-Ralph, M.: Lateralization of ventral and dorsal auditory-language pathways in the human brain. NeuroImage **24** (2007) 656–666

[10] Sepasian, N., Vilanova, A., Florack, L., ter Haar Romeny, B.: A ray tracing method for geodesic based tractography in diffusion tensor. Workshop on Mathematical Methods in Biomedical Image Analysis (MMBIA) (2008) 1–6

[11] Sepasian, N., ten Thije Boonkkamp, J., Vilanova, A., ter Haar Romeny, B.: Multi-valued geodesic based fiber tracking for diffusion tensor imaging. MICCAI 2009, Diffusion modeling and the fiber cup workshop (1) (2009) 6–13

[12] Kao, C.Y., Osher, S., Tsai, Y.H.: Fast sweeping methods for static hamilton–jacobi equations. SIAM J. Numer. Anal. **42**(6) (2004) 2612–2632

[13] Astola, L.J., Florack, L.M.J., ter Haar Romeny, B.M.: Measures for pathway analysis in brain white matter using diffusion tensor imaging. In Proceeding of Information Processing in Medical Imaging, Lecture Notes in Computer Science (2007) 642–649

[14] Wedeen, V., Davis, T., Weisskoff, R., Tootell, R., Rosen, B., Belliveau, J.: White matter connectivity explored by MRI. In Proceedings of the First International Conference for Functional Mapping of the Human Brain (1995)

[15] Evans, L.C.: Partial differential equations. American Mathematical Society **19** (1998)

[16] Ma, T., Tagare, H.: Consistency and stability of active contours with Euclidean and non-Euclidean arc-lengths. Biomedical Image Analysis, Workshop on **0** (1998) 1549–1559

[17] Rutherford, A.: Vectors, tensors and the basic equations of fluid mechanics (book). (1990)

[18] Rund, H.: The Hamilton-Jacobi theory in the calculus of variations : its role in mathematics and physics (book). (1966)

[19] Osher, S.: A level set formulation for the solution of the Dirichlet problem for Hamilton–Jacobi equations. SIAM Journal on Mathematical Analysis **24**(5) (1993) 1145–1152

[20] Mattheij, R.M.M., Rienstra, S.W., Ten Thije Boonkkamp, J.H.M.: Partial Differential Equations: Modeling, Analysis, Computation (Siam Monographs on Mathematical Modeling and Computation) (Saim Models on Mathematical Modeling and Computation). Society for Industrial and Applied Mathematics, Philadelphia, PA, USA (2005)

[21] Mantegazza, C., Mennucci, A.: Hamilton-Jacobi equations and distance functions on Riemannian manifolds. App. Math. and Optim. **47**(1) (2002) 1–25

[22] Runborg, O.: Mathematical models and numerical methods for high frequency waves. Communications in Computational Physics **2** (2007) 827–880

[23] Lenglet, C., Prados, E., Pons, J.P., Deriche, R., Faugeras, O.: Brain connectivity mapping using Riemannian geometry, control theory and PDEs. SIAM Journal on Imaging Sciences (SIIMS) **2**(2) (2009) 285–322

[24] Miller, E.N.: Icosahedra constructed from congruent triangles. Discrete Comput. Geometry **24** 437–451

[25] Kao, C.Y., Osher, S., Qian, J.: Lax-Friedrichs sweeping scheme for static Hamilton-Jacobi equations. J. Comput. Phys. **196**(1) (2004) 367–391

[26] Zhu, P., Zhou, S.: Relaxation Lax-Friedrichs sweeping scheme for static Hamilton-Jacobi equations. Numerical Algorithms (2000)

[27] Zhang, Y.T., Zhao, H.K., Chen, S.: Fixed-point iterative sweeping methods for static Hamilton-Jacobi equations. Methods Applied Analysis **13**(3) (2006) 299–320

[28] Zhao, H.K.: A fast sweeping method for eikonal equation. Mathematics of Computation **74**(250) (2003) 603–627

[29] Gremaud, P.A., Kuster, C.M.: Computational study of fast methods for the eikonal equation. SIAM J. Sci. Comput. **27**(6) (2006) 1803–1816

[30] Descoteaux, M., Lenglet, C., Deriche, R.: Diffusion tensor sharpening improves white matter tractography. In SPIE Medical Imaging **6512** (2007)

[31] Tournier, J.D., Calamante, F., Gadian, D.G., Connelly, A.: Diffusion-weighted magnetic resonance imaging fibre tracking using a front evolution algorithm. NeuroImage **20**(1) (2003) 276 – 288

[32] Pereyra, V., Lee, W.H.K., Keller, H.B.: Solving two-point seismic ray tracing problems in a heterogeneous medium. Bulletin of the Seismological Society of America **70** (1980) 79–99

[33] Motamed, M., Runborg, O.: A fast phase space method for computing creeping rays. Journal of Computational Physics **219**(1) (2006) 276–295

[34] Stejskal, E.O., Tanner, J.E.: Spin diffusion measurements: Spin echoes in the presence of a time-dependent field gradient. The Journal of Chemical Physics **42**(1) (1965) 288–292

[35] Wakana, S., Jiang, H., Nagae-Poetscher, L.M., van Zijl, P., Mori, S.: Fiber tract-based atlas of human white matter anatomy. Radiology **230**(1) (2004) 77–87

PREVIOUS PUBLICATIONS IN THIS SERIES:

Number	Author(s)	Title	Month
10-23	R. Choksi M.A. Peletier	Small volume fraction limit of the diblock copolymer problem: II. Diffuse-interface functional	Apr. '10
10-24	S. Adams N. Dirr M.A. Peletier J. Zimmer	From a large-deviations principle to the Wasserstein gradient flow: a new micro-macro passage	Apr. '10
10-25	P.I. Rosen Esquivel J.H.M. ten Thije Boonkkamp J.A.M. Dam R.M.M. Mattheij	Draft: Efficient estimation of the friction factor for forced laminar flow in axially symmetric corrugated pipes	May '10
10-26	J.C. van der Meer	Folding a cusp into a swallowtail	May '10
10-27	N. Sepasian A. Vilanova J.H.M. ten Thije Boonkkamp B.M. ten Haar Romeny	An innovative geodesic based multi-valued fiber-tracking algorithm for diffusion tensor imaging	May '10